

Department of Physics, Chemistry and Biology

Master's Thesis

Optical properties of free standing cubic silicon carbide

Mattias Jansson

Linköping, January 1, 2015

LiTH-IFM-EX--YY/NNNN--SE



Linköping University
INSTITUTE OF TECHNOLOGY

Department of Physics, Chemistry and Biology
Linköping University
SE-581 83 Linköping, Sweden

Optical properties of free standing cubic silicon carbide

Mattias Jansson

Linköping, January 1, 2015

Supervisor: **Jianwu Sun**
 IFM, Linköping University

Examiner: **Mikael Syvajarvi**
 IFM, Linköping University



Avdelning, Institution
Division, Department

Semiconductor physics
Department of Physics, Chemistry and Biology
SE-581 83 Linköping

Datum
Date

2015-01-01

Språk

Language

- Svenska/Swedish
 Engelska/English

Rapporttyp

Report category

- Licentiatavhandling
 Examensarbete
 C-uppsats
 D-uppsats
 Övrig rapport

ISBN

ISRN

LiTH-IFM-EX-YY/NNNN--SE

Serietitel och serienummer

Title of series, numbering

ISSN

URL för elektronisk version

<http://urn.kb.se/resolve?urn=urn:nbn:se:liu:diva-XXXXXX>

Titel

Optiska egenskaper för fristående kubisk kiselkarbid
Optical properties of free standing cubic silicon carbide

Författare

Mattias Jansson
Author

Sammanfattning

Abstract

If your thesis is written in English, the primary abstract would go here while the Swedish abstract would be optional.

Nyckelord

Keywords problem, lösning

Abstract

If your thesis is written in English, the primary abstract would go here while the Swedish abstract would be optional.

Contents

1	Introduction	1
2	An introduction to silicon carbide	3
2.1	Crystal structure	3
2.2	Band structure	4
2.3	Doping in 3C-SiC	7
2.3.1	Donors	7
2.3.2	Acceptors	8
3	Growth technique	11
3.1	About sublimation and nucleation	12
3.2	The sublimation growth setup	14
3.2.1	Doping using sublimation growth	15
4	Characterization techniques	17
4.1	Absorption measurements	17
4.2	Photoluminescence spectroscopy	18
4.3	Nomarski interference contrast microscopy	20
5	Experimental setup	23
5.1	Growth and sample preparation	23
5.2	Characterization experiments	24
6	Results	25
7	Discussion	31
8	Conclusion	33
9	Future work	35
	Bibliography	37

4

Characterization techniques

To investigate the material properties after growth, the samples must be characterized. There are many established techniques to do this. This chapter gives a description of the characterization techniques used to obtain the results in this thesis. This thesis focuses mainly on the optical properties of the grown samples, but the work also includes some morphology studies. The specifics of the experiments performed are given in chapter 5.

4.1 Absorption measurements

Absorption measurements are performed to find how much light is absorbed or transmitted when it hits the sample. In this way the band structure can be found even for samples with little or no luminescence. During measurements, light of different wavelengths hits the sample, some of which is absorbed and some is transmitted. The transmitted light passes through a spectrometer which measures the light intensity as a function of the wavelength. By measuring the light intensity before (I_0) and after (I) the sample, it is possible to compute the logarithm of the ratio of the two, which constitutes the *absorption* of the sample, i.e.

$$A(\lambda) = \log \left(\frac{I_0(\lambda)}{I(\lambda)} \right). \quad (4.1)$$

Generally some wavelengths are absorbed more than others. In semiconductors, light is absorbed to allow electrons to make a transition from a lower to a higher energy level. The band structure determines which transitions are allowed and which are not. Absorption of a certain wavelength means that there is an allowed transition with the same energy. The energy and wavelength relate through the formula

$$E = \frac{hc}{\lambda}, \quad (4.2)$$

where h is Planck's constant and c is the speed of light.

From absorption measurements it is also possible to find the absorption coefficient. This is done by using the Beer-Lambert law of transmission:

$$I = I_0 e^{-\alpha L}. \quad (4.3)$$

Where α is the absorption coefficient and L is the thickness of the sample. Combining this with equation 4.1 we can find the absorption coefficient. This is done by

$$I = I_0 e^{-\alpha L} \implies \log\left(\frac{I_0}{I}\right) = \alpha L \log(e),$$

which gives

$$\alpha = \frac{A}{L \log(e)}. \quad (4.4)$$

Having found the absorption coefficient it is also possible to find the effective band gap from the absorption data. This is done by the means of a *Tauc plot* [23]. In this method, the abscissa and ordinate of a plot contain the quantities hv and \sqrt{ahv} respectively, where v is the frequency of the light. If the data is obtained from an indirect semiconductor performing an allowed electron transition, then a part of the graph will be linear. Extrapolating this linear function to the energy axis will yield the band gap.

4.2 Photoluminescence spectroscopy

Photoluminescence (PL) spectroscopy is a very powerful tool in optical characterization of semiconductors. It is a non-invasive and fast technique. PL is similar to absorption spectroscopy in that a light source is aimed at the sample to induce electron excitations. As the electrons deexcite (recombine with holes), a photon is emitted. These emitted photons are called the *luminescence* of the sample, and is what is measured in PL spectroscopy. Figure 4.1 shows a schematic of the method of generating luminescence. As the laser beam (A) hits the sample (B), photoluminescence (C) is generated. As not all laser light is absorbed, some of the light reflects away from the sample (D).

The process of excitation and recombination is shown in figure 4.2, where a photon is captured (a) and generates an *electron hole pair (EHP)* (b). The EHP then recombines and emits a photon of energy corresponding to the band gap, E_g (c).

To generate an EHP by a transition between the valence and conduction bands, the energy of the light must be greater than the band gap. This is in accordance with the principle of conservation of energy. The laser must be chosen accordingly. Not only the energy is conserved in this process, but as is the momentum. Since SiC is an indirect semiconductor (see figure 2.3), an electron moving across the band gap has a change in momentum. The light momentum is far too small to compensate for this change. To allow the EHP to be generated, the change in momentum is contributed by phonons. As the transition occurs, a phonon is either created or annihilated. The phonon energies for the different modes in 3C-SiC are described in section 2.2. The

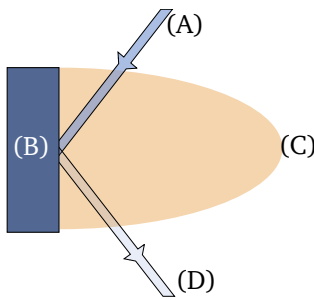


Figure 4.1: Photoluminescence induced from a sample by a laser beam.

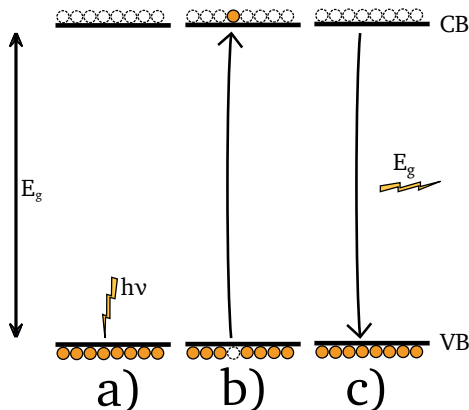


Figure 4.2: An EHP is generated by capture of a photon with energy $h\nu$ (a), (b). The EHP recombines to emit a photon of energy E_g .

phonons show in PL spectra as lines with energies slightly smaller than the value of the actual energy transition, called the *zero phonon line* (ZPL). The phonon lines are called *phonon replicas*.

The phonon replica lines can be used to investigate the biaxial stress in the material. The PL intensity of the transverse optical and longitudinal acoustic modes should be the same if the material is without internal stress. Hence the ratio

$$\frac{I_{LA}}{I_{TO}}$$

should be near unity in good quality samples [15]. Here I_{LA} and I_{TO} are PL intensities of arbitrary units. The phonon lines can also be used to estimate the doping concentration of a dopant. Camassel et al. have introduced a method where the full width at half maximum (FWHM) value of the TA-line is used for this purpose.

If doping levels are introduced in the band structure, then transitions can occur between such levels and the bands. In this case there will be another set of ZPL and phonon replicas at the new transition energy. The band structure can thus be inferred

from the PL spectrum.

As the EHP are generated, the electron and hole will interact with each other through the Coulomb force if they are near enough to each other. Due to their charge difference, they will start to orbit each other. This is called the *exciton* quasiparticle. The energy of recombination of an exciton is slightly shifted from a normal recombination of a EHP due to the potential energy from the Coulomb interaction. At room temperature the thermal energy from the ambient is generally high enough to split the exciton into a free electron and hole, so the excitons are not seen in the PL spectrum. At very low temperatures there is not enough energy to split the exciton, so the PL spectrum shows this shift in the recombination energy attributed to the Coulomb interaction. Some excitons can freely move in the sample, but some excitons bind to impurities in the sample. There is a small energy difference in the free and bound excitons attributed to the binding energy to the impurity. It is thus possible to distinguish from the free and bound excitons in the PL spectrum. They show that the concentration of nitrogen donors in the sample is proportional to the FWHM, Γ , through the formula

$$\Gamma_{\text{TA}} = A[N]^{1/n}. \quad (4.5)$$

Here A and n are constants and [N] denotes the concentration on nitrogen donors. This method has however not been validated for acceptor type impurities.

The PL setup can be described as follows. An optical setup is used to focus a laser beam on a sample. The emitted photoluminescence passes through another optical setup and is focused into a spectrometer. The spectrometer separates the incident light by wavelength, generally by the use of a grating. Photons with a given wavelength can now be collected by a photomultiplier tube or a CCD camera, and the photon intensity for the wavelength spectrum can be computed. Light is captured during a set time (generally ranging between seconds to minutes depending on the sample and setup).

The sample can be placed in a cryostat to measure the luminescence at low temperature, or measurements can be performed in room temperature. Various types of cryostats exist, generally using either liquid nitrogen or helium. In this work results have been obtained using room temperature measurements and by the use of a liquid helium cryostat.

4.3 Nomarski interference contrast microscopy

Nomarski interference contrast microscopy, also known as differential interference contrast microscopy, is a version of an optical microscope designed to be able to investigate the inside of samples. The method utilizes the polarization of light to give slightly different light paths depending on where in the sample the light passes. The setup is shown in figure 4.3.

The light is initially unpolarized. After passing a 45° polarization filter, the light enters a Wollaston prism. This prism will split the light in different directions depending on the polarization, creating two diverging beams. One beam will have light polarized in 0° direction and the other in the 90° direction. These two beams are focused on the sample by a lens, but made to hit the sample at slightly different

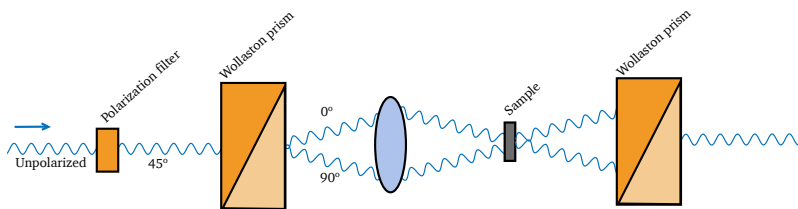


Figure 4.3: A schematic of the Nomarski microscope setup. The light passes through the setup from the left to the right.

positions. This will give the light beams slightly different paths through the sample. As the beams leave the sample they will enter another Wollaston prism, which will merge the two beams into one, and give the beams the same polarization, 135° . If the beams have travelled different lengths in the sample, or if the sample composition has varied between the two paths, then the beams will be slightly out of phase. This phase difference will lead through interference between the beams lead to optical contrast.

One possible use for the Nomarski microscope is to detect different thickness in the sample. It can also be used to detect different sample composition, if the compositions have different refractive indexes. As an example if a 3C-SiC sample has hexagonal inclusions, then these will give contrast in the microscope since the hexagonal and cubic polytypes have different refractive indexes.

5

Experimental setup

In this chapter, the experimental setup details are explained. The chapter is divided into two parts. The first part describes how the samples were grown and prepared. The second part describes details on the experimental setups for the characterization experiments.

5.1 Growth and sample preparation

All samples used in this work are grown using sublimation growth, as described in section 3.2. The nominally undoped samples are grown using two layers of XXX mm thick polycrystalline SiC source material. 4H-SiC substrates with 4° off axis surface were used for undoped growth. The substrates were chemically cleaned before growth. Typical size of the substrates were approximately 10 x 10 mm, and the thickness was XXX mm. Both the carbon and the silicon face of the 4H-SiC substrates were used during growth of undoped samples.

The doped samples were grown using either direct or indirect doping methods, as described in section 3.2.1. The source material for doped growth was doped polycrystalline SiC, doped with boron concentrations of 10^{18} , 10^{19} or 10^{20} cm⁻³. This was used together with a piece of undoped source material. The doped samples were grown either homoepitaxially on an undoped seed, or heteroepitaxially on the silicon face of a 4H-SiC substrate.

A piece of tantalum foil was placed in the bottom of the crucible for use as a carbon getter during growth of all samples. The source and substrate or seed were separated by a 1 mm thick graphite spacer for all samples. The substrate was held in place on the spacer by a graphite plate placed on top. All samples were grown at pressures in the order of 10^{-4} to 10^{-5} mbar, varying during the growth process. A vacuum pump was connected to the reactor and running continuously during growth. The temperature and growth time were varied between samples, and are given for

individual samples in section 6. The temperature was changed by varying the power supplied by the RF generator to the copper coil. The reactor setup is described further in section 3.2. Care was taken to place the insulating foam containing the crucible in the same position in the reactor for each run.

After growth the reactor was cooled in vacuum, by instantly setting the RF-generator to 0 W when the growth time was over. Cooling time was reduced by the use of a fan placed outside of the reactor. Optical microscopy images were done on samples as grown, but any other characterization was done after chemically cleaning the samples.

5.2 Characterization experiments

The absorption measurements were done with a PerkinElmer Lambda 950 UV/VIS setup. The software used was PerkinElmer UV WINLAB for molecular spectroscopy. Measurements were done in the range between 2000 to 380 nm. Samples were mounted on a black cardboard piece with a hole for light to pass through. Two hole sizes were used: XXX and YYY mm in diameter. Most samples were measured after mechanical polishing of the substrate, i.e. free-standing, but some samples were measured with the substrate remaining. The wavelength resolution of the spectrometer was 5 nm.

Low temperature photoluminescence measurements were performed using a liquid helium cryostat. The helium was supercooled to 2.6 K using a pump. The wavelength resolution of the setup was approximately 0.5 Å. A laser of wavelength XXX was used.

6

Results

In this chapter, the results of the experiments are shown. The results are further discussed in chapter 7.

Table 6.1: Growth conditions of seeds of undoped 3C-SiC grown on the carbon face of the substrate. For samples grown using a two stage temperature ramp up, the temperatures and growth times for each step are both shown.

	Temperature [°C]	Time [h:min]	Sample thickness [μm]	Terrace coverage [%]
#1	1825	4:00	700	40
#2	1850/1925	0:30/1:00	800	20
#3	1850/1925	0:30/1:00	800	
#4	1850/1925	0:30/1:00	900	30
#5	1875/1925	0:15/1:00	800	50
#6	1925	1:00	700	20
#7	1925	1:00	700	

To investigate growth of seeds to be used for B-doping, seeds were grown on both carbon and silicon face of the 4H-SiC. Table 6.1 shows the growth conditions and properties of the seeds grown on carbon face. The sample thickness is excluding the substrate thickness. Terrace coverage indicates the percentage of the step flow terrace covered by 3C-SiC rather than any other polytype. Not all sample coverages were measured quantitatively, but the percentages in the table are after initial examination of micrographs of the other samples thought to be representative. The silicon face seeds were all grown at temperatures 1850/1925 °C during times of 0:30/1:00 (hours/minutes). Nine out of ten of the silicon face grown seeds had a terrace coverage of 100 %, whereas none of the carbon face samples had complete terrace coverage.

The terrace coverage was estimated from optical micrographs

Figures 6.1 and 6.2 show representative micrographs of the terrace of carbon face grown seed #5. Figure 6.1 shows a reflection mode micrograph. It can clearly be seen that there are a few large areas of different polytypes. The hexagonal polytype regions show spiral growth, which on carbon face 4H-SiC manifests as a star shape. The 3C-SiC regions look much smoother, and show some of the characteristic triangle shapes. Figure 6.2 shows a Nomarski mode micrograph, showing clear contrast between the different polytype regions.

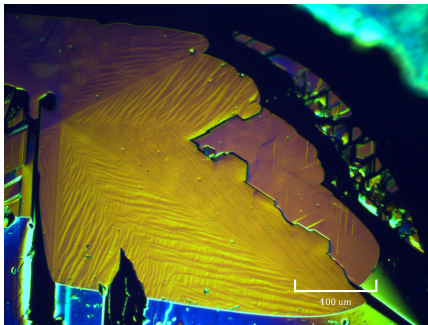


Figure 6.1: Reflection mode micrograph of the facet of C-face seed #5.

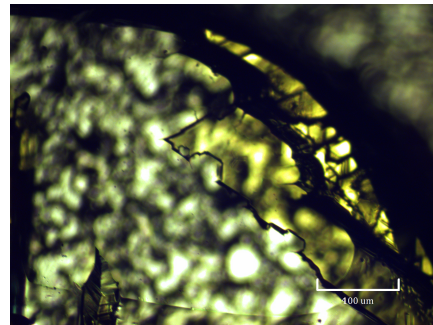


Figure 6.2: Nomarski transmission mode micrograph of the facet of C-face seed #5.

Table 6.2 shows the growth conditions and sample thickness of the grown B-doped samples. The thickness is measured for the doped layer, excluding both the substrate and the undoped seed. The growth mode is the stacking order of the doped and undoped source materials in the crucible, as described in section 3.2.1.

Table 6.2: Growth conditions of the doped samples are shown in this table. The growth mode describes which samples are grown using direct or indirect doping methods. These methods are described in section 3.2.1. The doping concentration is given for the source material.

	Temperature [°C]	Time [h:min]	Thickness [μm]	Doping [cm^{-3}]	Mode
#1	X	X:XX	X	10^{18}	Direct
#2	1825	2:30	350	10^{18}	Direct
#3	1825	3:00	360	10^{18}	Direct
#4	X	X:XX	440	10^{19}	Direct
#5	1825	2:30	320	10^{19}	Direct
#6	X	X:XX	X	10^{20}	Direct
#7	1825	2:30	220	10^{20}	Direct
#8	1825	2:30	380	10^{18}	Indirect
#9	1825	2:30	380	10^{20}	Indirect

Figure 6.3 shows the surface morphology of an undoped sample (a), doped sample number #1 (b), doped sample number #8 (c). The depicted area is chosen to

be an area with among the fewest defects possible. It is clearly seen that the undoped sample has a better crystal quality compared to the doped ones. This result was a trend with all grown samples. It should be noted that (b) and (c) show a directly and indirectly doped sample respectively.

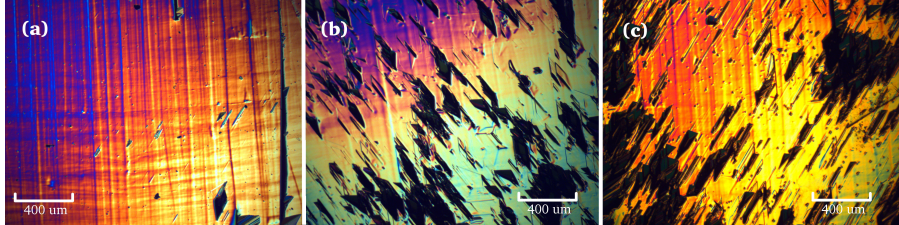


Figure 6.3: Micrographs of an undoped sample (a), doped sample number #1 (b) and doped sample number #8 (c).

Figure 6.4 (a)-(c) shows micrographs of samples #1, #4 and #6 respectively. It should be noted that these samples are grown using a source material doped with dopant concentration of 10^{18} , 10^{19} and 10^{20} cm^{-3} respectively. From the figures it can be seen that (a) and (b) have a significant density of defects on the surface. Figure (c) shows the smoothest surface, but some defects can still be seen.



Figure 6.4: Micrographs of doped samples with increasing source doping concentration. Figures (a)-(c) show samples #1, #4 and #6 respectively.

Figure 6.5 shows a transmission mode micrograph of sample #9. It can be seen that there are two different polytypes in the sample. The brighter area in the center is a foreign polytype inclusion.

Absorption measurements were done on directly doped samples with different source doping concentrations, samples #1 and #5. The results of these measurements are shown in figure 6.6, together with a reference spectrum from an undoped sample (dotted line). In both samples we see the VB to nitrogen transition at around 500 nm. A second feature in the doped sample spectra is the peak at around 700 nm, corresponding to the transition between the boron and nitrogen levels. This cannot be seen in the undoped sample. The doped samples show no evidence for a VB to boron transition, which should be seen at around 1800 nm, as described in chapter 2.3. Absorption was also measured for doped samples #6 and #7, but neither the band edge nor the boron related peaks was seen in these highly doped samples.

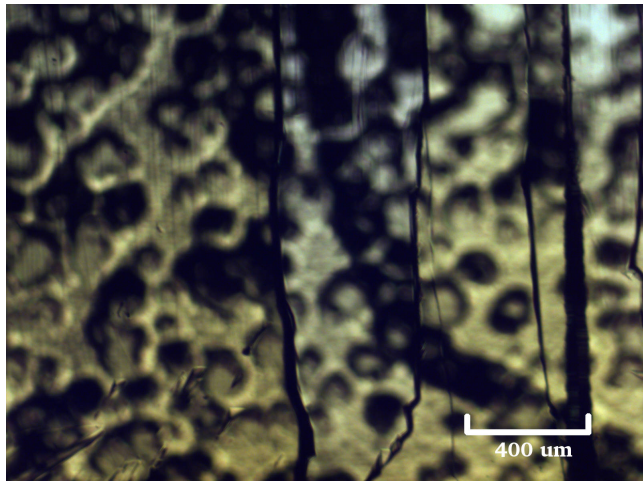


Figure 6.5: Transmission mode micrograph of doped sample #9. The brightness contrast shows a foreign polytype inclusion in the center.

Figure 6.7 shows the result of absorption measurements on samples #1 and #8, together with an undoped sample. It should be noted that #8 is an indirectly doped sample. It can be seen that both the doped sample spectra show the same trend. The graphs increase up to a point near the 700 nm B-N transition energy, where they level out. This is not visible in the undoped sample. It can further be seen that sample #8 has its B-N maximum at a slightly shorter wavelength compared to sample #1.

LTPL-measurements were done on boron doped samples and on an undoped seed. Figure 6.8 shows the resulting spectrum of the undoped seed. Five peaks can clearly be seen in the spectrum, labeled as ZPL and phonon replicas. It should be noted that the ZPL is significantly smaller than the phonon replicas. It can further be seen that several smaller peaks appear on the low energy side of the phonon replicas. These lines originate from exciton complexes.

As described in chapter 4.2, the strain in a crystal can be estimated by the fraction between the LA and TO lines. From figure 6.8 this is found to be

$$I_{\text{LA}}/I_{\text{TO}} = 0.783.$$

From the TA-line FWHM, the donor concentration can be found. The FWHM is found to be $\Gamma_{\text{TA}} = 1.094 \text{ meV}$, giving a nitrogen concentration of

$$[N] \approx 10^{16} \text{ cm}^{-3}.$$

Doped samples #1, #4 and #6 were measured using LTPL. Not one of these samples show any luminescence. Sample #9 did show luminescence, and the spectrum is shown in figure ??.

<Figure>.

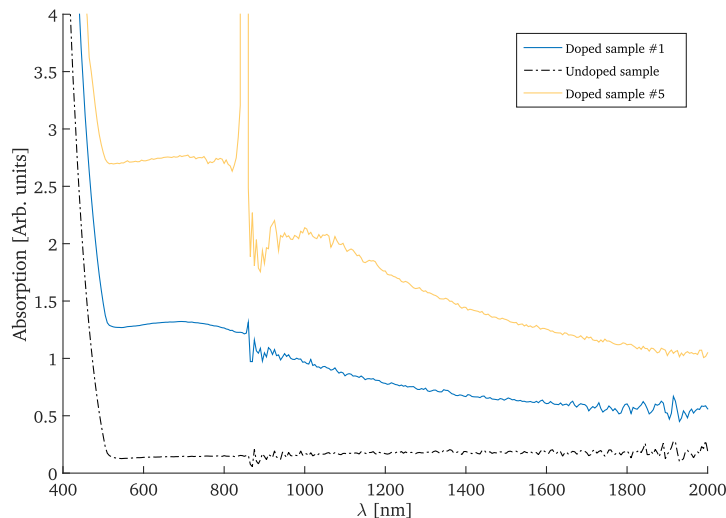


Figure 6.6: Absorption spectrum of undoped sample (dotted line), doped sample #5 (bright yellow line) and doped sample #1 (dark blue line).

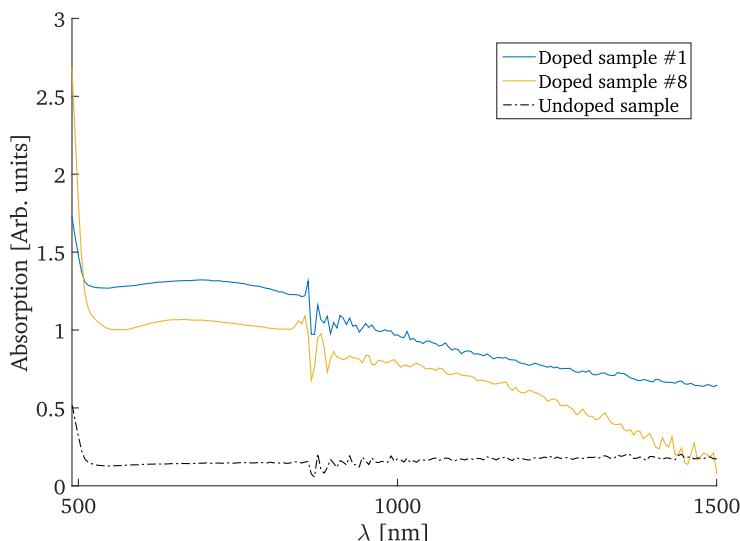


Figure 6.7: Absorption spectrum of doped samples #8 (bright yellow line) and #1 (dark blue line), shown together with an undoped sample (dotted line).

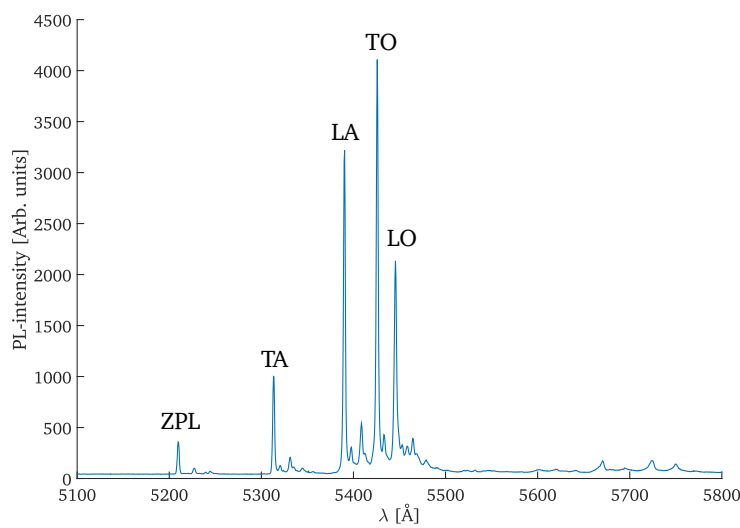


Figure 6.8: LTPL spectrum of an undoped seed. The five main peaks are labeled as ZPL and phonon replicas.

7

Discussion

In this chapter I will discuss the results of the work.

8

Conclusion

The conclusions drawn from this work are described here.

9

Future work

In this chapter I will write some of my thought of what is to be done in the future concerning these topics.

Bibliography

- [1] E.G. Acheson. Carborundum: Its history, manufacture and uses. *Journal of the Franklin Institute*, 136:279–289, 1893.
- [2] D N Hume and I M Kolthoff. The Silicon Carbide Electrode. *Journal of the American Chemical Society*, 63:2805–2806, 1941.
- [3] R. W. Johnson J. B. Casady. STATUS OF SILICON CARBIDE (SiC) AS A WIDE-BANDGAP SEMICONDUCTOR FOR HIGH-TEMPERATURE APPLICATIONS: A REVIEW. *Solid-State Electronics*, 39(10):1409–1422, 1996.
- [4] Valdas Jokubavicius, G Reza Yazdi, Rickard Liljedahl, Ivan G Ivanov, and Rositsa Yankova. Lateral Enlargement Growth Mechanism of 3C-SiC on Off-Oriented 4H-SiC Substrates. *Crystal growth and design*, 2014.
- [5] B.S. Richards, a. Lambertz, R.P. Corkish, C.a. Zorman, M. Mehregany, M. Ionescu, and M.a. Green. 3C-SiC as a future photovoltaic material. *3rd World Conference on Photovoltaic Energy Conversion, 2003. Proceedings of*, 3:2738–2741, 2003.
- [6] Masashi Kato, Tomonari Yasuda, Keiko Miyake, Masaya Ichimura, and Tomoaki Hatayama. Epitaxial p-type SiC as a self-driven photocathode for water splitting. *International Journal of Hydrogen Energy*, 39(10):4845–4849, March 2014.
- [7] Tomonari Yasuda, Masashi Kato, and Masaya Ichimura. Characterization of Photoelectrochemical Properties of SiC as a Water Splitting Material. *Materials Science Forum*, 717-720:585–588, May 2012.
- [8] Rebecca Cheung. *Silicon Carbide Microelectromechanical Systems Systems for Harsh Environments*. Number February. London, GBR: Imperial College Press, 2006.
- [9] a. P. Mirgorodsky, M. B. Smirnov, E. Abdelmounîm, T. Merle, and P. E. Quintard. Molecular approach to the modeling of elasticity and piezoelectricity of SiC polytypes. *Physical Review B*, 52(6):3993–4000, 1995.
- [10] D. Bimberg, M. Altarelli, and N.O. Lipari. A calculation of valence band masses, exciton and acceptor energies and the ground state properties of the electron-hole liquid in cubic SiC. *Solid State Communications*, 40:437–440, 1981.
- [11] H Aourag, B Djelouli, A Hazzab, and B Khelifa. Pseudopotential calculations on 3C-SiC. *Materials Chemistry and Physics*, 0584(94), 1994.

- [12] Richard Dalven. Temperature coefficient of the energy gap of β -silicon carbide, 1965.
- [13] K Karch, P Pavone, W Windl, O Schütt, and D Strauch. Ab initio calculation of structural and lattice-dynamical properties of silicon carbide. *Physical Review B*, 50(23):17054–17064, 1994.
- [14] J. a. Freitas, S. G. Bishop, P. E. R. Nordquist, and M. L. Gipe. Donor binding energies determined from temperature dependence of photoluminescence spectra in undoped and aluminum-doped beta SiC films. *Applied Physics Letters*, 52(20):1695, 1988.
- [15] Jianwu Sun, Ivan Gueorguiev Ivanov, Rickard Liljedahl, Rositsa Yakimova, and Mikael Syväjärvi. Considerably long carrier lifetimes in high-quality 3C-SiC (111). *Applied physics letters*, 100(252101), 2012.
- [16] Mulpuri V. Rao, J. Tucker, O. W. Holland, N. Papanicolaou, P. H. Chi, J. W. Kretchmer, and M. Ghezzo. Donor ion-implantation doping into SiC. *Journal of Electronic Materials*, 28(3):334–340, 1999.
- [17] P a Ivanov and V E Chelnokov. Recent developments in SiC single-crystal electronics. *Semiconductor Science and Technology*, 7:863–880, 1999.
- [18] Shigehiro Nishino, J. Anthony Powell, and Herbert a. Will. Production of large-area single-crystal wafers of cubic SiC for semiconductor devices. *Applied Physics Letters*, 42(1983):460–462, 1983.
- [19] Hiroyuki Nagasawa, Kuniaki Yagi, and Takamitsu Kawahara. 3C-SiC hetero-epitaxial growth on undulant Si(001) substrate. *Journal of Crystal Growth*, 237-239:1244–1249, 2002.
- [20] J. A. Lely. Darstellung von Einkristallen von Silicium Carbid und Beherrschung von Art und Menge der eingebauten Verunreinigungen. *Berichte der Deutschen Keramischen Gesellschaft*, 32:229–236, 1955.
- [21] H. J. Scheel and T. Fukuda. *Crystal growth technology*. Wiley, 2003.
- [22] Remigijus Vasiliauskas, Maya Marinova, Philip Hens, Peter Wellmann, Mikael Syväjärvi, and Rositsa Yakimova. Nucleation control of cubic silicon carbide on 6H-substrates. *Crystal Growth and Design*, 12:197–204, 2012.
- [23] J. Tauc. Optical properties and electronic structure of amorphous Ge and Si. *Materials Research Bulletin*, 3:37–46, 1968.